JOURNAL OF MATERIALS SCIENCE 29 (1994) 4700–4707

Structural studies of active carbon used in the growth of silicon carbide catalyst support

M. BENAISSA, J. WERCKMANN, G. EHRET
Groupe Surfaces-Interfaces, IPCMS, UMR 46 du CNRS, Université Louis Pasteur, 23 Rue du Loess, Bât. 69, 67037 Strasbourg Cedex, France

E. PESCHIERA, J. GUILLE, M. J. LEDOUX*
*Groupe des Matériaux Inorganiques, IPCMS, UMR 46 du CNRS, EHICS, and *Laboratoire de Chimie des Matériaux Catalytiques, 1 Rue Blaise Pascal, 67008 Strasbourg Cedex, France*

The microstructure of active carbon used in the growth of a silicon carbide catalyst support has been studied by BET area measurements, electron diffraction and high-resolution electron microscopy. The microstructure of the active carbon is consistent with different distributions of basic structural units (BSUs). These BSUs increase in size under heat treatment by forming adjacent distorted columns. Ordering processes are discussed from geometrical considerations based on reciprocal patterns. The reactivity of the interface between the active carbon and SiO vapour is controlled by the proportion of the highly reactive sites in the active carbon surface structure.

1. Introduction

Silicon carbide (SiC) ceramic powder is one of the most important catalyst supports recently used to replace the alumina support in heterogeneous catalysis [1–4]. The preparation method of our SiC ceramic powder [2] is based on the attack of high specific surface area (SSA) active carbon (Fluka, (Puriss) Activated Charcoal; C = 89.4%, H = 1.1%, O = 9.5%. SSA = 1150–1200 $m^2 g^{-1}$) by silicon monoxide (SiO) vapour at 1240 °C.

Typically, the SiC formed has high SSA (60–400 $m^2 g^{-2}$). The growth and microstructure of this material, which determines its catalytic and physical properties, has been previously studied by high-resolution transmission electron microscopy [5].

The SiC ceramic powder formation is described as follows: a SiO vapour is generated by heating, to a temperature of 1240 °C, an equimolar mixture of silicon and silica powders according to the reaction

$$Si + SiO_2 \rightleftharpoons 2SiO \quad (1)$$

The SiO then passes through a porous active carbon bed and reacts with it to form SiC according to the reaction

$$SiO + 2C \rightleftharpoons SiC + CO \quad (2)$$

The optimal reaction time, which determines the best yield of SiC, is about 7 h.

A complete conversion of the active carbon into silicon carbide has never been obtained. The main reason responsible for this is that the effect of heat treatment on the active carbon structure results in a decrease in the conversion rate. Because of the importance of the active carbon on the carbide growth, a detailed study of its microstructure is needed. However, let us first briefly recall the structure of carbonaceous materials.

Carbon has two strictly crystalline forms: diamond and graphite. In addition, carbon can also take on a number of partially crystalline forms ranging continuously from a nearly amorphous to a highly crystalline state [6]. Except for diamond, all carbonaceous materials are indexed as graphitizing or non-graphitizing carbons [7]. Various techniques, such as infrared [8] and Raman [9] spectroscopies, X-ray diffraction [10] and electron microscopy [11, 12], have been used to characterize the graphitization process of the carbonaceous materials. It was found that basic structural units (BSUs) [7] are formed first in the carbonization process. With increasing heat treatment up to 1000 °C, the material will release oxygenated (e.g. H_2O, CO_2, etc.) and hydrogenated (such as hydrocarbons) functions. This allows adjacent BSUs to get close enough to each other to form distorted columns. When heated above 1500 °C, adjacent columns get hooked to one another, edge to edge, forming distorted wrinkled layers. By heating up to 3000 °C, graphitizing carbons convert into graphite. Even for temperatures above 3000 °C, non-graphitizing carbons cannot achieve a final degree of graphitization as high as graphitizing carbons, because their elemental domains are much smaller [7].

Whereas the structure of graphite is accurately known (the three-dimensional unit cell is conventionally taken with four atoms at (0, 0, 0), (0, 0, 1/2), (2/3, 1/3, 0) and (1/3, 2/3, 1/2) with $c/a = 2.73$ and SG = $P6_{3/m}mc$), the structure of other carbonaceous materials is not well known. One structure reported in the

0022–2461

carbon literature is turbostratic carbon (TC) [13]. Unlike graphite, the hexagonal basal planes of carbon are not regularly stacked, but randomly rotated around the c-axis. The spacing between the basal planes in TC is larger than that in graphite, probably because of some interstitial atoms between the planes [14, 15] or because of the weak van der Waals force between basal planes because the structure of TC consists of random stacking sequences [16].

In this paper, we present the results of a TEM study, carried out in the selected-area diffraction (SAD) and high-resolution (HRTEM) modes, on the changes induced in the structure of the active carbon by heat treatment with and without SiO. Because the SSA can provide useful information about porosity and disorder, BET [17] measurements and pore-size distributions will be presented first.

2. Experimental procedure

The active carbon investigated in this study was heated under reduced pressure (0.5–0.8 torr) for 7 h at 1240 °C in the upper part of a reactor. Next, a mixture of Si–SiO_2 was reacted at the same temperature in the lower part of the same reactor. The SiO generated vapour is then pumped towards the upper part of the reactor where it reacts with the active carbon [2].

The SSA values given in this paper were determined by BET analysis of the adsorption isotherm of nitrogen at 77 K using a Micromeritics ASAP2000 porosimeter, which was capable of measuring pore sizes down to 2 nm.

HRTEM was carried out on a Topcon EM002B UHR electron microscope operating at 200 keV. All the micrographs were taken near the Scherzer defocus conditions. The selected aperture of the samples covered by the SAD was about 80 μm. Samples were ground between glass plates and brought into contact with a holey carbon-coated copper grid. The magnification of the HRTEM images, the electron diffraction patterns, and the optical diffractograms, were all calibrated under the same electron-optical conditions.

3. Results

3.1. BET and porosimetry

3.1.1. Heat-treated active carbon

Active carbon is characterized by its strong adsorption capacity which occurs mostly in micropores, which are smaller than 2.5 nm in size. This mainly determines its reactivity.

Nitrogen adsorption–desorption isotherms corresponding to untreated and heat-treated active carbon samples show that while the former does not show any difference between the adsorbed and the desorbed volume of nitrogen, the latter shows a hysteresis loop indicating the presence of slit pores [18, 19]. BET measurements carried out before and after heating indicate that the SSA decreased from 766 $m^2 g^{-1}$ to 500 $m^2 g^{-1}$ (Table I). Measurements of the pore-size distribution in the two active carbon samples (untreated and heat-treated) are illustrated in Fig. 1. Additional pores centred around 3.57 nm in size are seen in the heat-treated active carbon (dotted line). We thus conclude that these additional pores are slit pores which form during the heating process. The fact that the pore size increases and the SSA decreases as a result of heat treatment is probably linked to a structural reorganization of the active carbon structure.

TABLE I

Specimen[a]	BET ($m^2 g^{-1}$)
AC (before HT)	766
AC (after HT)	500
SiC + remaining AC (before calcination)	184
SiC (after calcination)	38
Remaining AC	338

[a] AC, active carbon; HT, heat treatment.

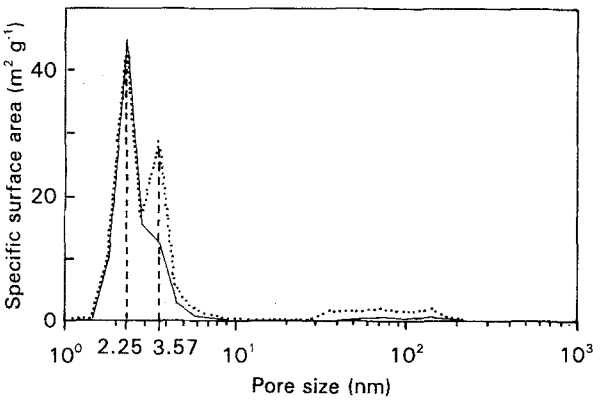

Figure 1 Pore-size distribution in (——) untreated and (···) heat-treated active carbons (AC).

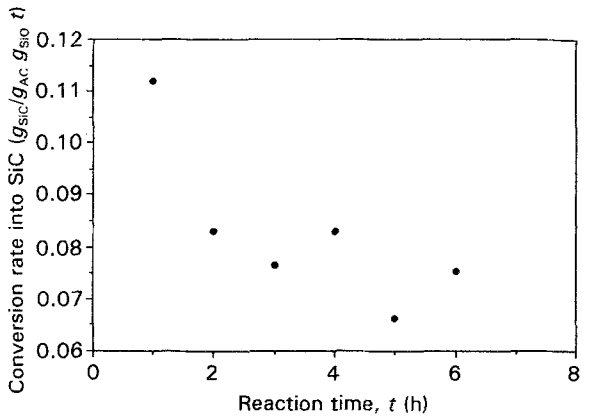

Figure 2 Variation of the conversion rate of active carbon into SiC during a 7 h reaction time. (The quantities g_{AC} and g_{SiO} represent the weight of reacted active carbon and SiO, respectively.)

3.1.2. Changes in the presence of SiO

Fig. 2 shows the conversion rate of active carbon into silicon carbide in the presence of SiO, versus reaction time. Note that the conversion rate decreases as the reaction time increases. One possible explanation is that the untreated active carbon becomes less reactive with increasing reaction time. The BET SSA measurements of the whole product (SiC plus remaining active carbon) after a 7 h reaction time gives a mean value

of 184 $m^2 g^{-1}$. The microporosity in pores centred around 2.25 and 3.57 nm is then strongly reduced compared to the heat-treated active carbon (Fig. 3, solid line) and nearly disappears after calcination of the product in air at 800 °C (Fig. 3, dotted line). Actually, calcination consists of the removal of remaining active carbon in order to determine the silicon carbide yield. It is worth noting that the BET value of the non-reacted (or remaining) active carbon has a lower value than that of the heat-treated active carbon. Indeed, the calculated BET SSA corresponding to the nonreacted active carbon is 338 $m^2 g^{-1}$. The reason for this is that the BET value calculated after reaction concerns only the structurally organized active carbon affected by the heat treatment which cannot react with SiO and consequently has a lower SSA.

3.2. Electron diffraction studies

3.2.1. Heat-treated active carbon

The SAD pattern of the untreated active carbon is shown in Fig. 4. The SAD of the heat-treated active carbon shows a similar pattern but with sharper rings (Fig. 5). Clearly, these reciprocal space pattern changes have to be explained in terms of the real space structure of the active carbon.

In order to explain these structural changes, an array of carbon atoms in a basal plane of graphite of infinite extent is considered first (Fig. 6a). The corresponding Fourier transform, which gives the reciprocal net, consists of two sets of six infinite lines normal to XY or xy (Fig. 6c). The first set, which corresponds to the "10" family of diffraction lines, has a radius length r_{10} and the second one, corresponding to the "11" family has a radius length r_{11} with $r_{11} > r_{10}$. If an infinite number of parallel basal layers rotated at arbitrary angles around 0Z is considered (Fig. 6b), the reciprocal lattice consists of concentric cylinders as shown in Fig. 6d. The innermost cylinder corresponds to the "10" diffraction surface while the next one corresponds to the "11" surface. But, assume now that the interplanar spacing among all the basal layers is equal; this will give rise to a set of reciprocal lattice points (0 0 0 l) normal the layers plane. Finally, the complete reciprocal lattice consists of a set of points (0 0 0 l) on the axis normal to the basal layers, i.e. 0Z,

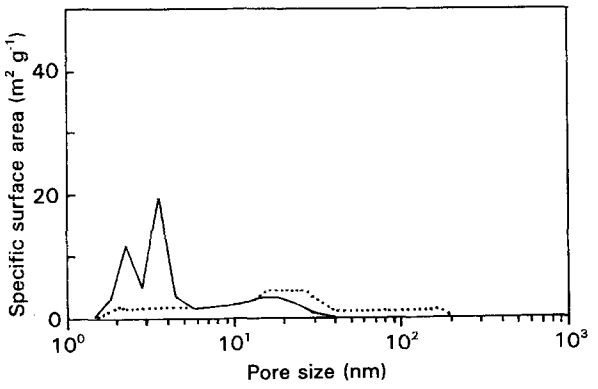

Figure 3 Pore-size distribution after a 7 h reaction time (——) before and after (····) calcination in air at 800 °C.

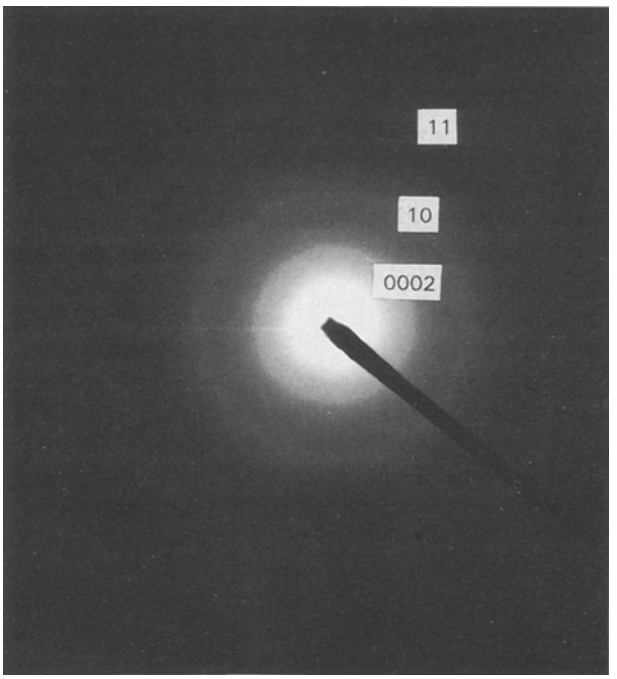

Figure 4 SAD diffraction pattern corresponding to the untreated active carbon.

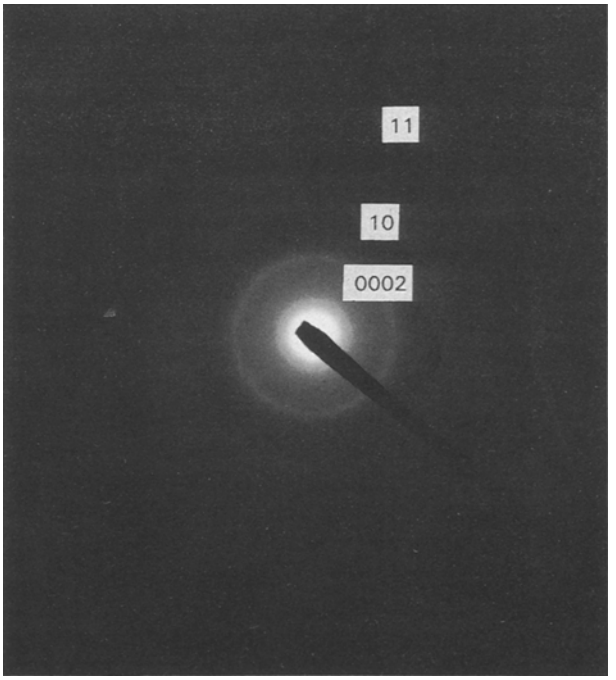

Figure 5 SAD diffraction pattern corresponding to the heat-treated active carbon.

surrounded by a set of concentric cylinders ($h k$) of increasing radius with axes along 0Z. The diffraction pattern is obtained by the intersection of the Ewald sphere with the reciprocal lattice. If the electron beam is considered parallel to 0Z, the electron diffraction pattern will consist of two rings namely "10" and "11" (Fig. 6e). An extra effect is also likely to occur if the stacking of basal planes is random. The interplanar spacing could be variable and depend on their relative orientation. Actually, the interplanar spacings are expected to peak around some average value slightly

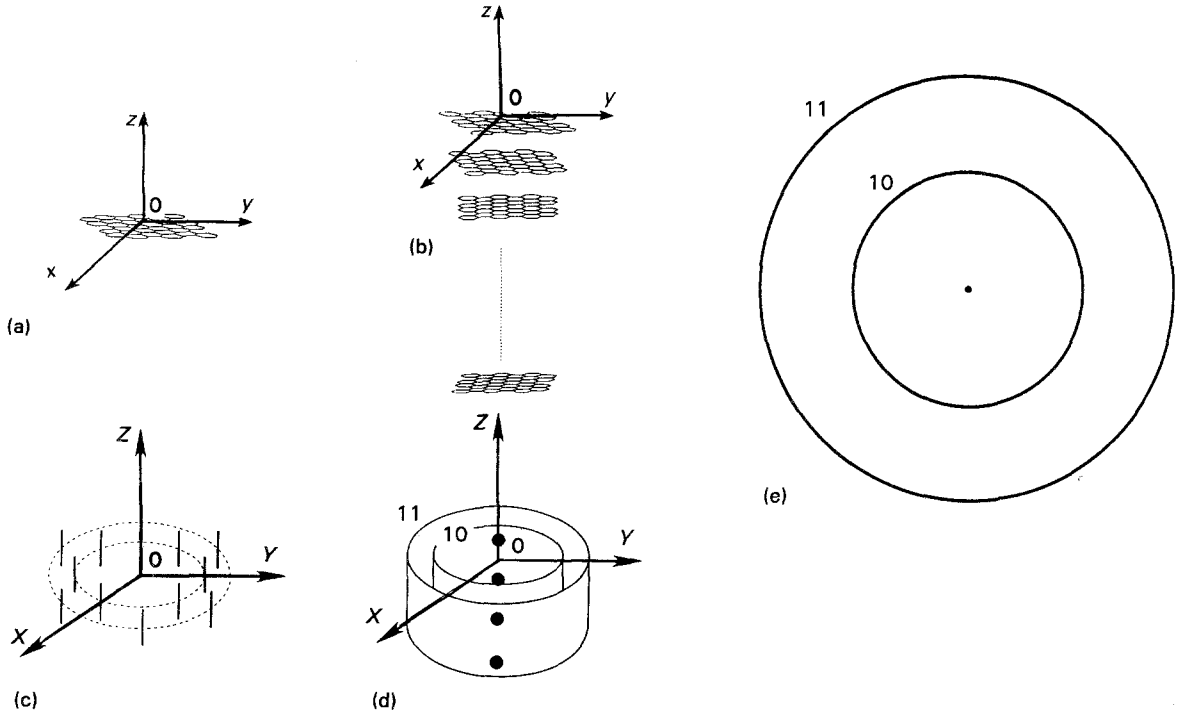

Figure 6 Real-space representations of (a) one layer of carbon atoms, and (b) an infinite number of carbon atoms layers rotated at random. The corresponding reciprocal space representation are given in (c) and (d), respectively. Electron diffraction pattern obtained for situation (b) in the case of an electron beam parallel to $0Z$ is given in (e).

larger than the graphitic spacing. This results in a slight broadening of the diffraction spots into diffraction discs (diffuse spots).

In the case of a finite number (3–10) of basal planes containing a limited number of carbon atoms each, the package can be described as a BSU according to Oberlin's model [7]. The geometry of the diffraction pattern will then roughly stay the same as before except that the diffraction spots will change into larger diffuse ones because of the Scherrer effect [20]. Considering an aggregate of a number of BSUs which are in parallel orientation with respect to each other, the diffuse diffraction spots will become sharp spots as the number of BSUs in the aggregate increases. If the BSUs are not in parallel orientation and have a misorientation angle with respect to each other (tilts around $0X$ and $0Y$), the concentric cylinders ($h\,k$) and the lattice points ($0\,0\,0\,l$) also rotate by the same angles. In the case of various tilt angles ranging from 0°–180°, the diffraction pattern results in a powder pattern having broadened rings. This is basically what is observed in Fig. 4. Because of their small size, the BSUs in the untreated active carbon have high misorientation angles resulting in randomly rotated aromatic carbon layers. Consequently, the interplanar spacings values are larger than the graphitic ones. After heat treatment, the width of the rings (especially (0 0 0 2)), shown in Fig. 5, is much smaller than the width of the pattern shown in Fig. 4. This indicates that the BSUs tend to reduce their misorientation angles with respect to each other. The interplanar spacings value approaches slightly the graphitic one. This results in a better stacking of the aromatic carbon layers and in an increase of the size of the coherent domains (i.e. the number of aromatic carbon layers per stack increases together with the 0 0 0 2 planar extension).

3.2.2. Changes in the presence of SiO

Fig. 7 shows the SAD pattern of an active carbon reacted with SiO at 1240 °C for 7 h. The SAD pattern consists of diffraction rings similar to those shown in the SAD pattern of Fig. 5 and additional spots,

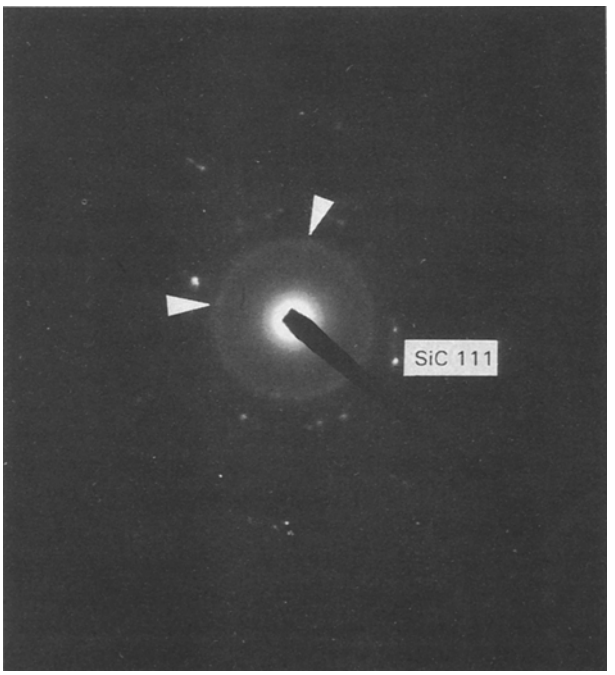

Figure 7 SAD diffraction pattern corresponding to the active carbon after 7 h reaction time with SiO.

marked as SiC (1 1 1), which correspond to the formed silicon carbide.

This result suggests that the non-reacted active carbon has undergone a similar structural organization to the heat-treated one. Considering the small width of the (0 0 0 2) diffraction ring, it seems that the structural organization of active carbon has improved. Some reflections are shown by arrows. In other words, the misorientation angle between the BSUs in that case is smaller than the one in the heat-treated active carbon without SiO. This is consistent with the HRTEM results as shown below.

3.3. HRTEM studies

3.3.1. Heat-treated active carbon

Fig. 8 shows a HRTEM micrograph of the untreated active carbon with the inset showing an optical diffractogram from the enlarged region. We observe that the structure consists of aromatic carbon layers randomly distributed. The size of the BSUs is very small and they do not show any preferred orientation. This is consistent with the SAD pattern of Fig. 5 which shows a diffuse continuous ring marked 0 0 0 2. Note that, in contrast to the electron diffraction pattern, the "10" and "11" rings do not appear in the optical diffractogram of Fig. 8. Indeed, because most of the BSUs are oriented parallel to the laser beam of the optical bench, the arrangement of atoms within the basal planes, which gives rise to the "10" and "11" rings, will not be present in the optical diffractogram.

Fig. 9 shows an HRTEM micrograph of the heat-treated active carbon and its optical diffractogram shown as an inset. The structure of the carbon consists of adjacent assemblies of piled BSUs. An improvement of parallelism of the carbon layers is clearly obvious from the micrograph. This is consistent with the sharpening of the (0 0 0 2) ring in the diffraction pattern of Fig. 5. The pair of arcs seen in the inset (Fig. 9) is due to the preferred orientation of the BSUs in the domain where the optical diffractogram has been recorded from.

3.3.2. Changes in the presence of SiO

Fig. 10 shows a HRTEM micrograph of the remaining active carbon found in a SiC sample. It is immedi-

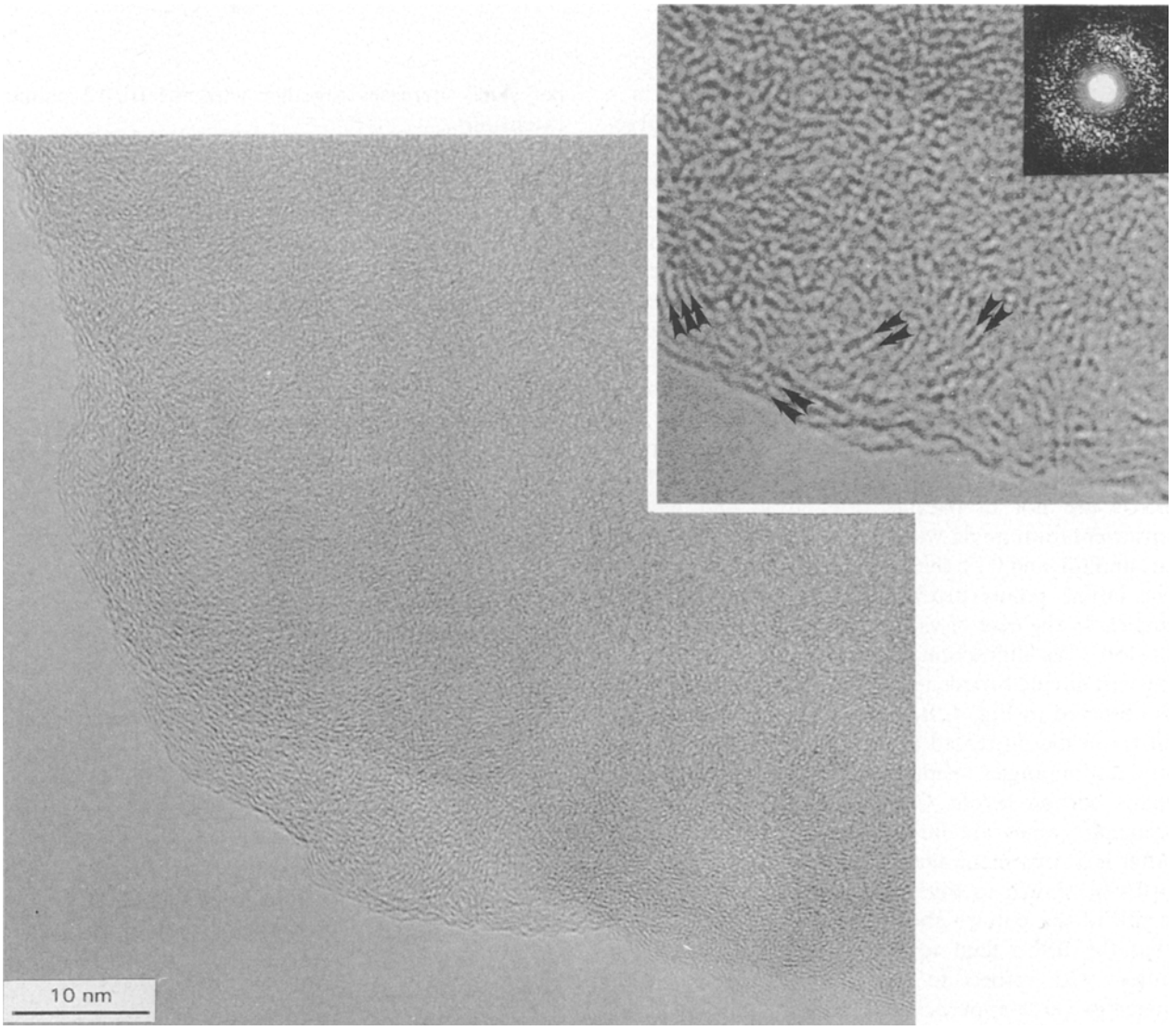

Figure 8 HRTEM micrograph of the untreated active carbon. The arrows show some parallel carbon sheets considered as small BSUs. The optical diffractogram is shown at the upper right side of the enlarged area.

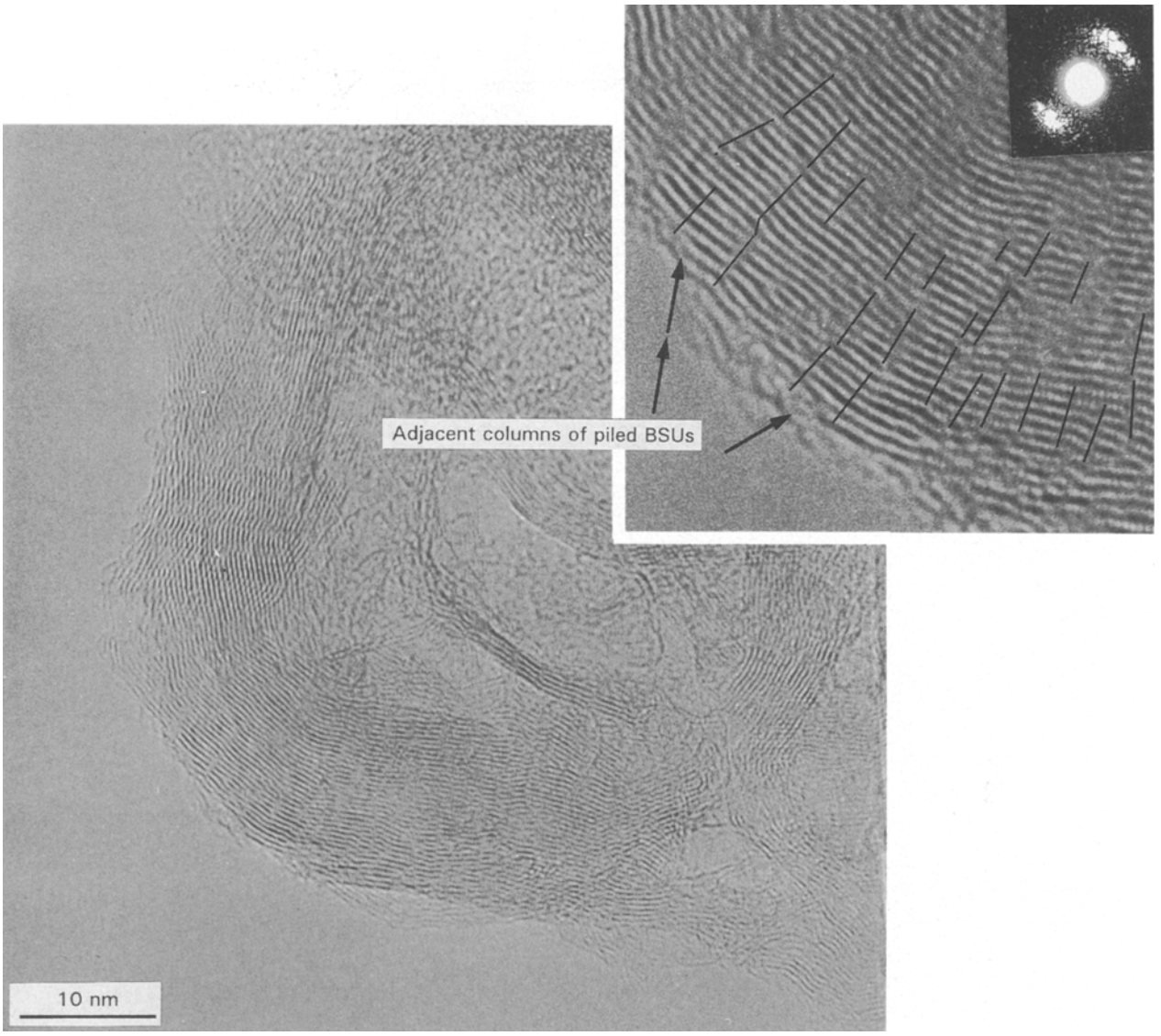

Figure 9 HRTEM micrograph of the heat-treated active carbon. The optical diffractogram is shown at the upper right side of the enlarged area.

ately apparent from the micrograph that notable structural changes have taken place, the regions of parallel layers formed having an average spacing of 0.346 nm. From Fig. 10, it follows that basal planes have reached a high degree of parallelism, i.e. the number of aromatic carbon layer per stack has increased together with the 0002 planar extention, as compared to the heat-treated active carbon without SiO. This demonstrates the improvement in ordering gained by heat treatment in the presence of SiO. It can also be seen that the different domains, containing the well-stacked BSUs, are randomly distributed. This random distribution, together with the improvement of the stacking of the carbon layers, results in sharper rings in the diffraction pattern of Fig. 7.

4. Discussion

Our results show that the misorientation angle between the BSUs in the active carbon is more reduced in the case of heat treatment with than without SiO. This suggests that in addition to the heat-treatment effect, the carbide formation may also have an influence on the non-reacted active carbon. The structural differences between the HRTEM micrographs (Figs 8 and 9) indicate that ordering processes during heat treatment occur predominantly within existing BSUs. An improvement in ordering is expected because there will be a concomitant release of strain energy within different adjacent columns resulting in the formation of domains having preferred orientations. This decrease in the misorientation angle between the BSUs closes up the micropores that form the main contribution to the SSA of the active carbon. Consequently, the graphene layers grow and new slit pores are formed. The characteristic curvature (Fig. 9) is indicative of the high density of defects which must be present between adjacent columns of piled BSUs. There is evidence from the high degree of the alignment (Fig. 10) that internal defects within the layer planes are fewer in number in the presence of SiO. However, some degree of disorder is present at the extremities of the oriented domains. These disordered extremities have been described as couples of highly distorted planes having interlayer spacing in the range 0.4–1.25 nm [21].

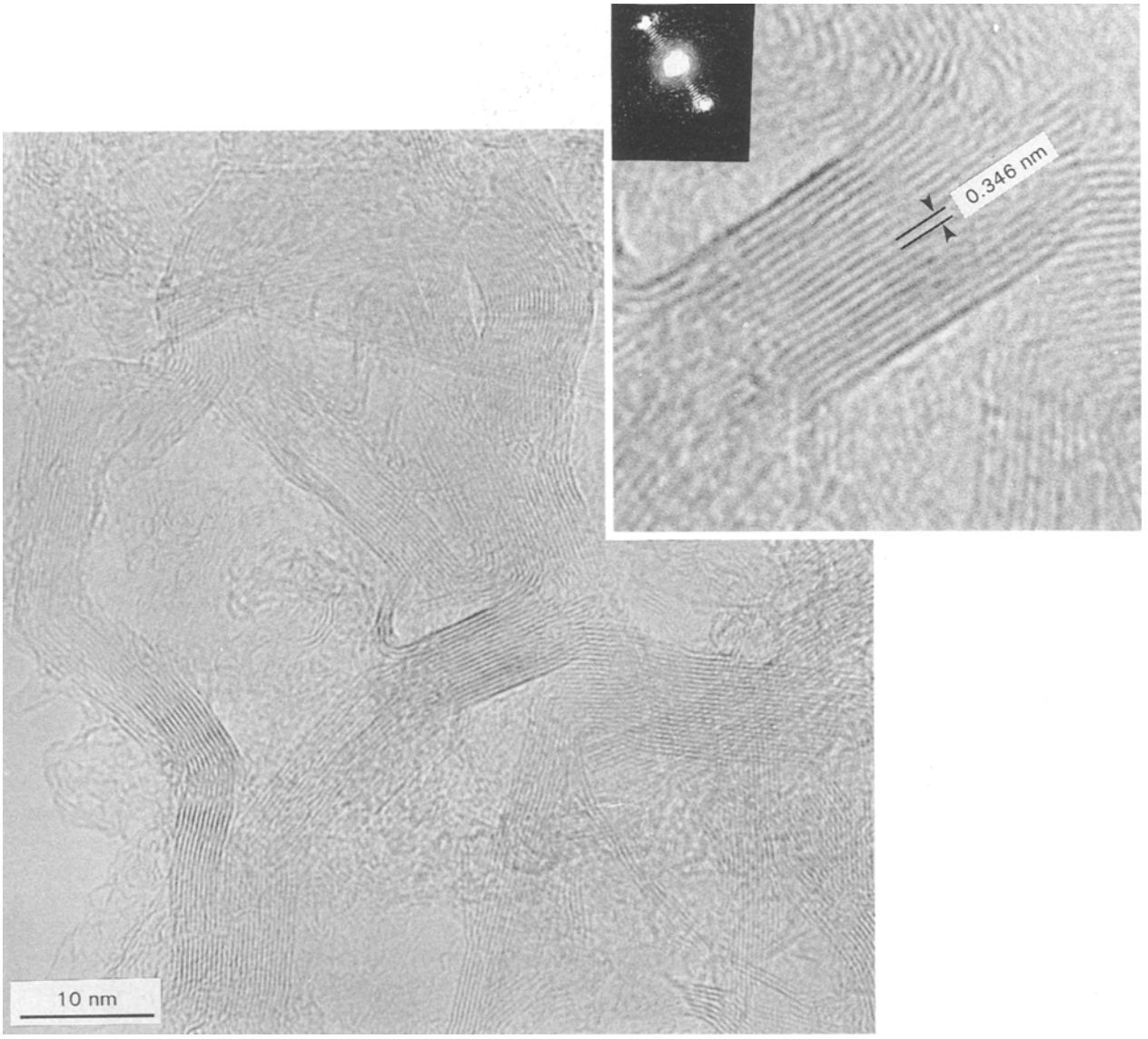

Figure 10 HRTEM micrograph of the unreacted active carbon. The optical diffractogram is shown at the upper left side of the enlarged area.

Considering a BSU (block ranging from 1–2 nm in size and containing three or four parallel carbon sheets [22]) as a small block of TC, the active carbon surface may have three structural forms, namely a basal plane, represented by a relatively inactive (0 0 0 1) plane, a first prism plane with carbon atoms oriented in a "zig-zag" pattern, represented by (1 0 $\bar{1}$ 0) planes, and a second prism plane in an "armchair" orientation, represented by (1 1 $\bar{2}$ 0) planes. In the case of graphite, the specific surface energy of the basal plane and of the prism plane are reported to be 0.14 and 4.8 J m^{-2}, respectively [23]. This implies that the reactivity at the interface of active carbon with SiO will mainly depend on the density of free edge carbon atoms in the reactive plane existing on the active carbon surface. The decrease of the conversion rate as the reaction proceeds (Fig. 2) can be explained from the difference of the crystalline structure of the active carbon surface. Indeed, BSUs constituting the active carbon are small in size and spatially distributed at random. Therefore, the proportion of reactive sites of the highly reactive prism plane exposed at the active carbon surface is greater in the first stage of the reaction and will rapidly chemisorb SiO molecules. This provides random nucleation sites for silicon carbide in the active carbon matrix [5] during and immediately after infiltration. During reaction, the active carbon is heated to 1240 °C, the BSUs reduce their misorientation angle by ordering processes and preferred orientation domains grow (Fig. 10). As the reaction time increases, ordering processes occur within BSUs by removing the functional groups, thereby reducing the number of surface reactive sites in these domains, while the SiO molecule will preferentially react with a disordered active carbon. This growth mode will affect the conversion rate because the well-organized active carbon does not react with SiO.

5. Conclusion

Our studies on active carbon under conditions pertinent to SiC formation using BET area measurements, electron diffraction and high-resolution electron microscopy show the following conclusions. The microstructure of the active carbon can be explained

in terms of different assemblies of BSUs. The interpretation of diffraction patterns and HRTEM micrographs showed that the BSUs increase in size on heat treatment by forming domains of preferred orientations. The reactivity at the interface between the active carbon and the SiO vapour depends strongly on the number of highly reactive sites located at the prismatic planes exposed at the surface of the active carbon. During the reaction, the active carbon becomes structurally more organized and the number of reactive sites is decreased. This will have an incidence on the conversion rate to silicon carbide. This fact is confirmed by HRTEM micrographs which show that the remaining active carbon, which does not react with SiO vapour, has a highly organized structure.

References

1. M. J. LEDOUX, J. GUILLE, S. HANTZER and D. DUBOTS, Eur. Pat. 88-420352.
2. M. J. LEDOUX, S. HANTZER, C. PHAM-HUU, J. GUILLE and M. P. DESANEAUX, *J. Catal.* **114** (1988) 176.
3. K. C. TAYLOR, in "Catalysis and Automotive Pollution Control" (Studies in Surface Science and Catalysis, Vol. 30) edited by A. Crucq and A. Frennet (Elsevier, Amsterdam, 1987) p. 97.
4. M. BOUTONNET KIZLING, P. STENIUS, S. ANDERSSON and A. FRESTAD, *Appl. Catal. B: Environmental* **1** (1992) 149.
5. M. BENAISSA, J. WERCKMANN, J. L. HUTCHISON, E. PESCHIERA, J. GUILLE and M. J. LEDOUX, *J. Crystal Growth* **131** (1993) 5.
6. J. C. BUKROS, in "Chemistry and Physics of Carbon", Vol. 5 edited by P. L. Walker (Marcel Dekker, New York, 1969) p. 79.
7. A. OBERLIN, *Carbon* **22** (1984) 521.
8. P. ROUXHET, P. ROBIN and G. NICAISE, in "Technip", edited by B. Durand (Paris, 1982) p. 162.
9. F. TUINSTRA and J. KOENING, *J. Chem. Phys.* **53** (1970) 1126.
10. R. FRANKLIN, *Acta Crystallogr.* **3** (1950) 107.
11. A. OBERLIN, G. TERRIERE and J. BOULMIER, *J. Tanso Jpn* **80** (1975) 29.
12. *Idem, ibid.* **81** (1975) 153.
13. W. RULAND, in "Chemistry and Physics of Carbon," Vol. 4, edited by P. L. Walker (Marcel Dekker, New York, 1968) p. 67.
14. J. MAIRE and J. MERING, *ibid.*, Vol. 6 (Marcel Dekker, New York, 1970) p. 19.
15. M. HEGGIE, *Carbon* **30** (1) (1992) 71.
16. B. E. WARREN, *Phys. Rev.* **59** (1941) 693.
17. S. BRUNAUER, P. EMMATT and E. TELLER, *J. Am. Chem. Soc.* **60** (1938) 309.
18. S. GREGG and K. SING, "Adsorption, Surface Area and Porosity", (Academic Press, London, 1982).
19. A. LECLOUX, in "Exploitation des isothermes d'adsorption et de desorption d'azote pour l'étude de la texture des solides poreux", Extrait des mémoires de la Société Royale des Sciences de Liège, 6ième série, Vol. 1, fascicule 4 (1971) p. 169.
20. B. D. CULLITY, in "Elements of X-Ray Diffraction", 2nd Edn, edited by M. Cohen (Addison-Wesley, New York, 1978).
21. M. HUTTEPAIN and A. OBERLIN, *Carbon* **11** (1) (1990) 103.
22. A. OBERLIN, *J. Microsc. Spectrosc. Electron.* **7** (1982) 327.
23. J. ABRAHAMSON, *Carbon* **11** (1973) 337.

Received 16 September 1993
and accepted 7 March 1994